Effect of surface slip on Stokes flow past a spherical particle in infinite fluid and near a plane wall

Haoxiang Luo · C. Pozrikidis

Abstract The motion of a spherical particle in infinite linear flow and near a plane wall, subject to the slip boundary condition on both the particle surface and the wall, is studied in the limit of zero Reynolds number. In the case of infinite flow, an exact solution is derived using the singularity representation, and analytical expressions for the force, torque, and stresslet are derived in terms of slip coefficients generalizing the Stokes–Basset–Einstein law. The slip velocity reduces the drag force, torque, and the effective viscosity of a dilute suspension. In the case of wall-bounded flow, advantage is taken of the axial symmetry of the boundaries of the flow with respect to the axis that is normal to the wall and passes through the particle center to formulate the problem in terms of a system of one-dimensional integral equations for the first sine and cosine Fourier coefficients of the unknown traction and velocity along the boundary contour in a meridional plane. Numerical solutions furnish accurate predictions for (a) the force and torque exerted on a particle translating parallel to the wall in a quiescent fluid, (b) the force and torque exerted on a particle rotating about an axis that is parallel to the wall in a quiescent fluid, and (c) the translational and angular velocities of a freely suspended particle in simple shear flow parallel to the wall. For certain combinations of the wall and particle slip coefficients, a particle moving under the influence of a tangential force translates parallel to the wall without rotation, and a particle moving under the influence of a tangential torque rotates about an axis that is parallel to the wall without translation. For a particle convected in simple shear flow, minimum translational velocity is observed for no-slip surfaces. However, allowing for slip may either increase or decrease the particle angular velocity, and the dependence on the wall and particle slip coefficients is not necessarily monotonic.

Keywords Boundary-integral method · Particle motion · Stokes flow · Surface slip · Suspension

H. Luo
Department of Mechanical Engineering, Vanderbilt University, 2301 Vanderbilt Pl., Nashville, TN 37235-1592, USA
e-mail: haoxiang.luo@vanderbilt.edu

C. Pozrikidis (✉)
Department of Mechanical and Aerospace Engineering, University of California, San Diego, La Jolla, CA 92093-0411, USA
e-mail: cpozrikidis@ucsd.edu

1 Introduction

Gas flow in micro-electro-mechanical systems occurs at exceedingly small Reynolds numbers and under conditions where the ratio between the molecular mean free path and the boundary size, expressed by the Knudsen number, is no longer infinitesimal. Examples include flow in micro-reactors and minute heat exchangers in micro-electronics, DNA sequencing systems, and hand-held gas chromatography devices. Non-infinitesimal Knudsen numbers also arise in the flow around small aerosol particles and during the late stages of collision of particles with surfaces when the gap becomes comparable to the molecular mean free path. The discrete nature of the fluid under these circumstances is manifested, in part, as a defiance of the no-slip boundary condition normally assumed for non-rarefied gas flows. In various physical and engineering systems, the slip length may vary in size from nanometers to micrometers.

A liquid may also slide over a surface when the wall shear stress is high enough to overcome the fluid–solid molecular attraction forces, as it does near three-phase contact lines moving over a boundary. Although slip velocity has been reported in the flow of liquids over hydrophobic and possibly more general surfaces [1,2], the laboratory evidence is not conclusive. On the other hand, macromolecular solutions and melts are known to exhibit intermittent slip that may initiate flow instability [3]. In traditional engineering applications, slip occurs over the boundaries of porous materials (e.g., [4]).

The slip boundary condition was first proposed by Navier [5] and further discussed by Maxwell [6] in the context of gas flow [7,8]. Basset [9] derived an analytical solution for the flow due to a solid sphere translating in infinite fluid at low Reynolds numbers, and generalized the Stokes law for the drag force. In subsequent decades, although particle motion subject to the no-slip boundary condition has received an enormous amount of attention, only a few efforts have been made to describe the corresponding slip flows. Hocking [10] considered the motion of a sphere toward a plane wall or another sphere and showed that, when slip is allowed on both surfaces, the resistive force becomes only logarithmically dependent on the gap, and contact can be achieved at a finite time. His solution was subsequently generalized to account for different slip coefficients on the surfaces of the sphere and wall [11]. Other authors considered Stokes flow past a slip sphere using series expansions [12–14].

Keh and Chen [15] and Mohan and Brenner [16] generalized Faxen's laws for a spherical particle accounting for the slip velocity, and Wen and Lai [17] considered particle motion through a cylindrical tube. Palaniappan and Daripa [18] derived a family of two-dimensional Stokes flows inside a circular cylinder with the slip boundary condition applied. More recently, Elasmi and Feuillebois [19,20] and Lauga and Squires [21] derived the fundamental singularity of Stokes flow in a semi-infinite domain bounded by a plane wall where the slip boundary condition applies, and developed integral and asymptotic solutions.

In this paper, we consider the motion of a spherical particle in infinite fluid and near a plane wall, allowing for slip both over the particle surface and the wall. The particle may translate and rotate as a rigid body or be convected in an infinite linear flow or under the influence of a simple shear flow parallel to the wall. Our main goal is to compute resistance coefficients in the case of translation and rotation, and the translational and angular velocities in the case of free motion. The resistance coefficients for translation can be used to compute the diffusivity of small Brownian particles [21]. In the case of infinite flow, we seek a prediction for the effective viscosity of an infinite dilute suspension.

An exact solution for a linear ambient flow in an infinite domain will be presented in terms of Stokes-flow singularities. The analytical results generalize Basset's [9] formula for the force and furnish expressions for the torque and stresslet consistent with those derived by Felderhof and coworkers for arbitrary incident flows using Faxen's law combined with series expansions [12,13]. In the case of wall-bounded flow, the problem formulation relies on the boundary-integral method for Stokes flow, properly simplified to take advantage of the axial symmetry of the boundaries of the flow with respect to the axis that is normal to the wall and passes through the particle center. Implementing this simplification, we obtain a system of one-dimensional integral equations for the first Fourier coefficients of the unknown traction and velocity along the boundary contour in a meridional plane. The solution is found efficiently and accurately by boundary-element methods for gaps as small as 10^{-3} times the particle radius.

2 Linear flow past a spherical particle in an infinite domain

We consider infinite linear flow with velocity $\mathbf{u}^\infty = \mathbf{U} + \mathbf{A} \cdot \mathbf{x}$ past a translating and rotating spherical particle of radius a, where $\mathbf{U}$ is a constant velocity, and $\mathbf{A}$ is the transpose of the velocity gradient tensor, $\mathbf{A}^T = \nabla \mathbf{u}^\infty$. Mass conservation requires that the trace of $\mathbf{A}$ is zero. The Reynolds number written with respect to the particle size is assumed to be sufficiently small so that the motion of the fluid is governed by the equations of Stokes flow,

$$-\nabla p + \mu \nabla^2 \mathbf{u} = \mathbf{0}, \quad \nabla \cdot \mathbf{u} = 0, \tag{2.1}$$

where p is the pressure, $\mathbf{u}$ is the velocity, and μ is the fluid viscosity. The no-penetration and slip boundary conditions apply over the particle surface,

$$\mathbf{u} = \mathbf{V} + \mathbf{\Omega} \times (\mathbf{x} - \mathbf{x}_c) + \mathbf{u}^S, \tag{2.2}$$

where $\mathbf{V}$ is the velocity of translation of the particle center, $\mathbf{x}_c$, and $\mathbf{\Omega}$ is the angular velocity of rotation about $\mathbf{x}_c$. The first two terms on the right-hand side of (2.2) represent rigid-body motion. The slip velocity is given by the Navier–Maxwell–Basset formula

$$\mathbf{u}^S = \frac{a}{\mu \beta_p} \mathbf{f} \cdot (\mathbf{I} - \mathbf{nn}) = \frac{\lambda_p}{\mu} \mathbf{n} \times \mathbf{f} \times \mathbf{n}, \tag{2.3}$$

where $\mathbf{f} \equiv \boldsymbol{\sigma} \cdot \mathbf{n}$ is the traction, $\boldsymbol{\sigma}$ is the stress tensor, $\mathbf{n}$ is the unit normal vector pointing into the fluid, $\mathbf{I} - \mathbf{nn}$ is the tangential projection operator, and β_p is the dimensionless Basset particle-slip coefficient ranging from zero for vanishing shear stress and perfect slip, to infinity for finite shear stress and no-slip. In the case of perfect slip, the drag force is due exclusively to the form drag due to the pressure.

In rarified gases, the slip coefficient, β_p, and slip length, λ_p, can be rigorously related to the mean free path, λ_f, by the Maxwell relation $\lambda_f / \lambda = \beta_p Kn = \sigma / (2 - \sigma)$, where $Kn \equiv \lambda_f / a$ is the Knudsen number, and σ is the tangential momentum accommodation coefficient (TMAC) expressing the fraction of molecules that undergo diffusive instead of specular reflection (e.g., [7,8]). The limit $\sigma = 2$ yields the no-slip boundary condition, $\beta_p \to \infty$, whereas the limit $\sigma = 0$ yields the perfect-slip boundary condition, $\beta_p \to 0$.

For convenience, we set the particle center at the origin, $\mathbf{x}_c = \mathbf{0}$. Using the singularity representation (e.g., [22]), we express the velocity field in the form

$$u_i = U_i + A_{ij} x_j + a \, G_{ij} g_j + a^3 \Delta_{ij} d_j + a^3 R_{ij} \gamma_j + a^3 D_{ijl} \alpha_{jl} + a^5 Q_{ijl} \zeta_{jl}, \tag{2.4}$$

where G_{ij} is the Stokeslet representing a point force, Δ_{ij} is the potential doublet, R_{ij} is the rotlet representing a point couplet, D_{ij} is the Stokeslet doublet representing a point-force dipole, and Q_{ijl} is the potential quadrupole, given by

$$G_{ij} = \frac{\delta_{ij}}{r} + \frac{x_i x_j}{r^3}, \quad \Delta_{ij} = -\frac{\delta_{ij}}{r^3} + 3 \frac{x_i x_j}{r^5}, \quad R_{ij} = \epsilon_{ijl} \frac{x_l}{r^3},$$

$$D_{ijl} = \frac{\delta_{ij} x_l - \delta_{il} x_j - \delta_{jl} x_i}{r^3} + 3 \frac{x_i x_j x_l}{r^5},$$

$$Q_{ijl} = -3 \frac{\delta_{ij} x_l + \delta_{il} x_j + \delta_{jl} x_i}{r^5} + 15 \frac{x_i x_j x_l}{r^7}. \tag{2.5}$$

In these expressions, r is the distance from the particle center, δ_{ij} is Kronecker's delta representing the identity matrix, and g_j, d_j, γ_j, α_{jl}, and ζ_{jl}, are unknown singularity coefficients. Since Q_{ijl} is symmetric with respect to j and l, we can assume that ζ_{jl} is also symmetric.

The no-penetration boundary condition requires $u_i x_i = V_i x_i$ at $r = a$. Substituting the singularities and simplifying, we find

$$u_j x_j = U_j x_j + A_{jl} x_j x_l + 2 (g_j + d_j) x_j + (-\delta_{jl} a^2 + 3 x_j x_l)(\alpha_{jl} + 3 \zeta_{jl}) = V_j x_j, \tag{2.6}$$

and hence

$$\mathbf{g} + \mathbf{d} = -\frac{1}{2} (\mathbf{U} - \mathbf{V}), \quad \boldsymbol{\alpha}^S + 3 \boldsymbol{\zeta} = -\frac{1}{3} \mathbf{E}, \tag{2.7}$$

where the superscript S denotes the symmetric part of a tensor, and $\mathbf{E}$ is the rate-of-deformation tensor, $\mathbf{E} = \mathbf{A}^S$. The tangential component of the velocity is

$$u_i^| = u_i - u_m \frac{x_i x_m}{a^2} = U_i + A_{ij} x_j + a\, G_{ij}\, g_j + a^3\, \Delta_{ij}\, d_j + a^3\, D_{ijl}\, \alpha_{jl} + a^5\, Q_{ijl}\, \zeta_{jl} + a^3\, R_{ij}\, \gamma_j$$

$$- \frac{x_i x_m}{a^2} \left(U_m + A_{mj} x_j + a\, G_{mj}\, g_j + a^3\, \Delta_{mj}\, d_j + a^3\, D_{mjl}\, \alpha_{jl} + a^5\, Q_{mjl}\, \zeta_{jl} + a^3\, R_{mj}\, \gamma_j \right). \tag{2.8}$$

Making substitutions and simplifying, we find

$$u_i^| = (U_j + g_j - d_j)(\delta_{ij} - \frac{x_i x_j}{a^2}) + \epsilon_{ilj}\, \gamma_l\, x_j + (A_{ij} + \alpha_{ij} - \alpha_{ji} - 3\,\zeta_{ij} - 3\,\zeta_{ji})\, x_j$$

$$+ \frac{1}{a^2}\, (-A_{lj} + 6\,\zeta_{jl})\, x_i x_j x_l. \tag{2.9}$$

The stress field is given by

$$\sigma_{ik} = \mu \left(A_{ik} + A_{ki} + a\, \Sigma_{ijk}^G\, g_j + a^3\, \Sigma_{ijk}^\Delta\, d_j + a^3\, \Sigma_{ijk}^R\, \gamma_j + a^3\, \Sigma_{ijlk}^D\, \alpha_{jl} + a^5\, \Sigma_{ijlk}^Q\, \zeta_{jl} \right), \tag{2.10}$$

where

$$\Sigma_{ijk}^G = -6\, \frac{x_i x_j x_k}{r^5}, \quad \Sigma_{ijk}^\Delta = 6\, \frac{\delta_{ij}\, x_k + \delta_{ik}\, x_j + \delta_{jk}\, x_i}{r^5} - 30\, \frac{x_i x_j x_k}{r^7},$$

$$\Sigma_{ijlk}^D = 6\, \frac{\delta_{il}\, x_j x_k + \delta_{jl}\, x_i x_k + \delta_{kl}\, x_i x_j}{r^5} - 30\, \frac{x_i x_j x_l x_k}{r^7},$$

$$\Sigma_{ijlk}^Q = -6\, \frac{\delta_{ij}\, \delta_{kl} + \delta_{ik}\, \delta_{jl} + \delta_{jk}\, \delta_{il}}{r^5} + 30\, \frac{(\delta_{ij}\, x_k + \delta_{ik}\, x_j + \delta_{jk}\, x_i)\, x_l}{r^7}$$

$$+ 30\, \frac{\delta_{il}\, x_j x_k + \delta_{jl}\, x_i x_k + \delta_{kl}\, x_i x_j}{r^7} - 210\, \frac{x_i x_j x_l x_k}{r^9}, \tag{2.11}$$

$$\Sigma_{ijk}^R = 3\, \frac{\epsilon_{ilj}\, x_k + \epsilon_{klj}\, x_i}{r^5}\, x_l,$$

are the stress tensors of the individual singularities. Note that all of these tensors are symmetric with respect to i and k, as required.

The surface traction on the sphere is $f_i = \sigma_{ik} x_k / a$, and its tangential component is

$$f_i^| = f_i - f_m \frac{x_i x_m}{a^2} = \frac{\mu x_k}{a} \left(A_{ik} + A_{ki} + a\, \Sigma_{ijk}^G\, g_j + a^3\, \Sigma_{ijk}^\Delta\, d_j + a^3\, \Sigma_{ijk}^R\, \gamma_j + a^3\, \Sigma_{ijlk}^D\, \alpha_{jl} + a^5\, \Sigma_{ijlk}^Q\, \zeta_{jl} \right)$$

$$- \frac{\mu x_i x_m x_k}{a^3} \left(A_{mk} + A_{km} + a\, \Sigma_{mjk}^G\, g_j + a^3\, \Sigma_{mjk}^\Delta\, d_j + a^3\, \Sigma_{mjk}^R\, \gamma_j + a^3\, \Sigma_{mjlk}^D\, \alpha_{jl} + a^5\, \Sigma_{mjlk}^Q\, \zeta_{jl} \right). \tag{2.12}$$

Making substitutions and simplifying, we find

$$f_i^| = 6\mu\, d_j \left(\delta_{ij} - \frac{x_j x_i}{a^2} \right) + \frac{3\mu}{a}\, \gamma_l\, \epsilon_{ijl}\, x_j + \frac{\mu}{a}\, (A_{ij} + A_{ji} + 6\alpha_{ji} + 24\,\zeta_{ij} + 24\,\zeta_{ji} - 6\,\zeta_{kk}\delta_{ij})\, x_j$$

$$+ \frac{\mu}{a^3} (6\,\zeta_{kk} - 2A_{jl} - 6\alpha_{jl} - 48\,\zeta_{jl})\, x_i x_j x_l. \tag{2.13}$$

The slip boundary condition on the particle surface requires

$$u_i^| - V_i + V_m \frac{x_i x_m}{a^2} - \epsilon_{ijk}\Omega_j x_k = \frac{a}{\mu \beta_p}\, f_i^|. \tag{2.14}$$

Substituting the expressions for the tangential components of the velocity and traction and grouping similar terms, we find

$$\mathbf{U} - \mathbf{V} + \mathbf{g} - \mathbf{d} = \frac{6}{\beta_p}\, \mathbf{d}, \quad \boldsymbol{\gamma} = \frac{\beta_p}{\beta_p + 3}\, \boldsymbol{\Omega}, \tag{2.15}$$

and also

$$\mathbf{A} + 2\boldsymbol{\alpha}^A - 6\boldsymbol{\zeta} = \frac{1}{\beta_p}\, \left(2\,\mathbf{E} + 6\,\boldsymbol{\alpha}^T + 48\,\boldsymbol{\zeta} - 6\,\mathrm{Trace}(\boldsymbol{\zeta})\,\mathbf{I} \right),$$

$$(\beta_p - 2)\,\mathbf{E} - 6\boldsymbol{\alpha}^S - 6\,(8 + \beta_p)\,\boldsymbol{\zeta} + 6\,\mathrm{Trace}(\boldsymbol{\zeta})\,\mathbf{I} = \mathbf{0}, \tag{2.16}$$

where the superscript A denotes the antisymmetric part of a tensor, and the superscript T denotes the matrix transpose.

Combining the first equation in (2.7) with the first equation in (2.15), we find

$$\mathbf{g} = \frac{3}{4} \frac{\beta_p + 2}{\beta_p + 3} \, (\mathbf{V} - \mathbf{U}), \quad \mathbf{d} = \frac{1}{4} \frac{\beta_p}{\beta_p + 3} \, (\mathbf{U} - \mathbf{V}). \tag{2.17}$$

The force exerted on the sphere is

$$\mathbf{F} = -8 \, \pi \mu a \mathbf{g} = -6 \, \pi \mu a \, \frac{\beta_p + 2}{\beta_p + 3} \, (\mathbf{V} - \mathbf{U}), \tag{2.18}$$

in agreement with earlier analysis [9,12,13]. The parameter ξ used by Schmitz and Felderhof [13] is related to the Basset parameter, β, by $\xi = 1/(\beta + 3)$. As $\beta_p \to 0$, the Stokes-law coefficient of six tends to four, indicating a substantial reduction in the drag force.

Combining the second equation in (2.7) with Eqs. (2.16), we find

$$\boldsymbol{\alpha}^S = -\frac{5}{6} \frac{\beta_p + 2}{\beta_p + 5} \, \mathbf{E}, \quad \boldsymbol{\alpha}^A = -\frac{1}{2} \frac{\beta_p}{\beta_p + 3} \, \boldsymbol{\Xi}, \quad \boldsymbol{\zeta} = \frac{1}{6} \frac{\beta_p}{\beta_p + 5} \, \mathbf{E}, \tag{2.19}$$

where $\boldsymbol{\Xi}$ is the vorticity tensor, $\boldsymbol{\Xi} = \mathbf{A}^A$. Thus,

$$\boldsymbol{\alpha} = \boldsymbol{\alpha}^S + \boldsymbol{\alpha}^A = -\frac{(4\beta_p^2 + 20 \, \beta_p + 15) \, \mathbf{A} + (\beta_p^2 + 5 \, \beta_p + 15)\mathbf{A}^T}{6 \, (\beta_p + 3)(\beta_p + 5)}. \tag{2.20}$$

The coefficient of the couplet inherent in the antisymmetric part of the Stokeslet dipole is

$$L_m = -\epsilon_{mjl} \, a^3 \, \alpha_{jl}^A = \frac{1}{2} \, \epsilon_{mjl} \, a^3 \, \frac{\beta_p}{\beta_p + 3} \, A_{jl} = -\frac{a^3}{2} \, \frac{\beta_p}{\beta_p + 3} \, \omega_m^\infty, \tag{2.21}$$

where $\boldsymbol{\omega}^\infty$ is the vorticity of the linear flow. The torque exerted on the sphere is given by

$$\mathbf{T} = -8\pi \mu \, (a^3 \, \boldsymbol{\gamma} + \mathbf{L}) = -4\pi \mu a^3 \, \frac{\beta_p}{\beta_p + 3} \, (2 \, \boldsymbol{\Omega} - \boldsymbol{\omega}^\infty). \tag{2.22}$$

A torque-free particle thus rotates with an angular velocity that is equal to half the vorticity of the incident flow. When $\beta_p = 0$, a rotating particle does not generate a flow and the torque vanishes.

The coefficient of the stresslet is given by

$$\mathbf{S} = -8\pi \mu \, a^3 \, \boldsymbol{\alpha}^S = \frac{20}{3} \, \pi \mu a^3 \, \frac{\beta_p + 2}{\beta_p + 5} \, \mathbf{E}, \tag{2.23}$$

and the effective viscosity of a dilute suspension is given by

$$\mu_{\text{eff}} = \mu \, \left(1 + c \, \frac{5}{2} \, \frac{\beta_p + 2}{\beta_p + 5} \right), \tag{2.24}$$

where c is the particle volume fraction. This expression generalizes Einstein's formula for no-slip spheres, recovered in the limit $\beta_p \to \infty$. As $\beta_p \to 0$, the Einstein coefficient of 5/2 tends to unity, indicating a substantial reduction in the effective viscosity of an infinitely dilute suspension.

We have derived an exact solution for linear flow past a translating and rotating spherical particle. The results confirm our intuition that the slip velocity reduces the drag force, the torque, and the effective viscosity of a dilute suspension.

3 Particle motion near a plane wall

In the second part of this paper, we consider the motion of a spherical particle near an infinite plane wall under the action of an imposed simple shear flow (Fig. 1). The x-axis is perpendicular to the wall and passes through the
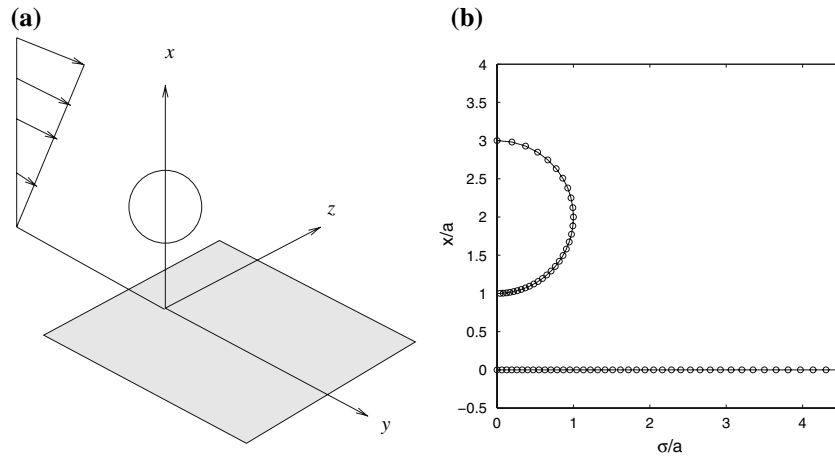
Fig. 1 (**a**) Illustration of a spherical particle near a planar wall in the presence of a simple shear flow. (**b**) Typical discretization of the particle and wall contour in an azimuthal plane

particle center, and the y points in the direction of the unperturbed shear flow. Far from the particle, the velocity field, designated by the superscript ∞, is given by $u_x^\infty = 0$, $u_z^\infty = 0$, and $u_y^\infty = kx$, where k is the shear rate. The coordinate system is convected in the y-direction with the wall-slip velocity corresponding to the unperturbed shear flow so that the wall-velocity appears to be zero. For simplicity, we assume that the particle is neutrally buoyant. The presence or motion of the particle generates a disturbance flow, denoted by the superscript D, that may be added to the simple shear flow to yield the total flow with velocity $\mathbf{u} = \mathbf{u}^\infty + \mathbf{u}^D$.

The no-penetration and slip boundary conditions prevail over the particle surface and the wall. Over the particle surface, we require the boundary condition (2.2) subject to the slip condition (2.3). Over the wall, we require the corresponding condition

$$\mathbf{u} = \frac{a}{\mu\beta_w}\,\mathbf{n} \times \mathbf{f}^D \times \mathbf{n} = \frac{\lambda_w}{\mu}\,\mathbf{f}^D \cdot (\mathbf{I} - \mathbf{nn}), \tag{3.1}$$

where β_w is a dimensionless wall slip coefficient, and $\lambda_w = a/\beta_w$ is the wall slip length.

3.1 Boundary-integral formulation

To compute the solution, we use the boundary-integral formulation for Stokes flow and express the disturbance velocity at the point $\mathbf{x}_0$ that lies inside the fluid in terms of integrals over the particle surface, P, and wall, W, as

$$\mathbf{u}^D(\mathbf{x}_0) = -\frac{1}{8\pi\mu}\,\boldsymbol{\mathcal{S}}(\mathbf{x}_0, \mathbf{f}, P) - \frac{1}{8\pi\mu}\,\boldsymbol{\mathcal{S}}(\mathbf{x}_0, \mathbf{f}^D, W) + \frac{1}{8\pi}\,\boldsymbol{\mathcal{D}}(\mathbf{x}_0, \mathbf{u}^S, P) + \frac{1}{8\pi}\,\boldsymbol{\mathcal{D}}(\mathbf{x}_0, \mathbf{u}, W). \tag{3.2}$$

We have introduced the single- and double-layer potentials of Stokes flow defined over a generic surface, D,

$$\mathcal{S}_j(\mathbf{x}_0, \mathbf{f}, D) \equiv \iint_D f_i(\mathbf{x})\,G_{ij}(\mathbf{x}, \mathbf{x}_0)\,\mathrm{d}S(\mathbf{x}),$$

$$\mathcal{D}_j(\mathbf{x}_0, \mathbf{u}, D) \equiv \iint_D u_i(\mathbf{x})\,T_{ijk}(\mathbf{x}, \mathbf{x}_0)\,n_k(\mathbf{x})\,\mathrm{d}S(\mathbf{x}), \tag{3.3}$$

where

$$G_{ij}(\mathbf{x}, \mathbf{x}_0) = \frac{\delta_{ij}}{r} + \frac{\hat{x}_i \hat{x}_j}{r^3}, \quad T_{ijk}(\mathbf{x}, \mathbf{x}_0) = -6\,\frac{\hat{x}_i \hat{x}_j \hat{x}_k}{r^5}, \tag{3.4}$$

are, respectively, the free-space Green's function and associated stress tensors, $\hat{\mathbf{x}} = \mathbf{x} - \mathbf{x}_0$, and $r = |\hat{\mathbf{x}}|$ (e.g., [22]). Note that the integral representation (3.2) involves the total traction and the slip velocity over the particle

surface. This has become possible through the application of the reciprocal identity for the simple shear flow over the particle volume, and the subsequent application of integral identities for the part of the boundary condition expressing rigid-body motion. Since in the chosen frame of reference the velocity of the simple shear flow is zero over the wall, the total velocity has been used instead of the disturbance velocity over the wall.

On the wall located at $x = 0$, the unit normal vector points along the x-axis, the x velocity component is zero due to the no-penetration boundary condition, and the double-layer potential takes the form

$$
\begin{aligned}
\mathcal{D}_j(\mathbf{x}_0, \mathbf{u}, W) &= -6\,\hat{x} \iint_W \frac{u_y\,\hat{y} + u_z\,\hat{z}}{[x_0^2 + \hat{y}^2 + \hat{z}^2]^{5/2}}\,(\mathbf{x} - \mathbf{x}_0)_j\,\mathrm{d}S(\mathbf{x}) \\
&= -6\,\hat{x} \iint_W \frac{u_\sigma\,(\sigma - \sigma_0 \cos\hat{\varphi}) + u_\varphi\,\sigma_0\,\sin\hat{\varphi}}{(x_0^2 + \sigma^2 + \sigma_0^2 - 2\sigma\sigma_0 \cos\hat{\varphi})^{5/2}}\,(\mathbf{x} - \mathbf{x}_0)_j\,\mathrm{d}S(\mathbf{x}),
\end{aligned}
\tag{3.5}
$$

where φ is the meridional angle, $\hat{\varphi} = \varphi - \varphi_0$, and σ is the distance from the x-axis. The associated cylindrical polar components are

$$
\begin{bmatrix} \mathcal{D}_x \\ \mathcal{D}_\sigma \\ \mathcal{D}_\varphi \end{bmatrix} (\mathbf{x}_0, \mathbf{u}, W) = -6\,\hat{x} \iint_W \frac{u_\sigma\,(\sigma - \sigma_0 \cos\hat{\varphi}) + u_\varphi\,\sigma_0\,\sin\hat{\varphi}}{(x_0^2 + \sigma^2 + \sigma_0^2 - 2\sigma\sigma_0 \cos\hat{\varphi})^{5/2}} \begin{bmatrix} \hat{x} \\ \sigma\cos\hat{\varphi} - \sigma_0 \\ \sigma\,\sin\hat{\varphi} \end{bmatrix} \mathrm{d}S(\mathbf{x}).
\tag{3.6}
$$

On the sphere, the double-layer potential takes the form

$$
\begin{aligned}
\mathcal{D}_j(\mathbf{x}_0, \mathbf{u}, P) &= -6 \iint_P \frac{u_x\,\hat{x} + u_y\,\hat{y} + u_z\,\hat{z}}{[\hat{x}^2 + \hat{y}^2 + \hat{z}^2]^{5/2}}\,(\mathbf{x} - \mathbf{x}_0)_j\,(\mathbf{x} - \mathbf{x}_0)\cdot\mathbf{n}(\mathbf{x})\,\mathrm{d}S(\mathbf{x}) \\
&= -\frac{6}{a} \iint_P \frac{u_x\,\hat{x} + u_\sigma\,(\sigma - \sigma_0 \cos\hat{\varphi}) + u_\varphi\,\sigma_0\,\sin\hat{\varphi}}{(\hat{x}^2 + \sigma^2 + \sigma_0^2 - 2\sigma\sigma_0 \cos\hat{\varphi})^{5/2}}\,(\mathbf{x} - \mathbf{x}_0)_j\,\mathcal{G}\,\mathrm{d}S(\mathbf{x}),
\end{aligned}
\tag{3.7}
$$

where $\hat{x} = x - x_0$, x_c is the x coordinate of the particle center, and $\mathcal{G} = (x - x_c)\,\hat{x} + \sigma\,(\sigma - \sigma_0 \cos\hat{\varphi})$. The associated cylindrical polar components are

$$
\begin{aligned}
\begin{bmatrix} \mathcal{D}_x \\ \mathcal{D}_\sigma \\ \mathcal{D}_\varphi \end{bmatrix} (\mathbf{x}_0, \mathbf{u}, P) &= -\frac{6}{a} \iint_P \frac{u_x\hat{x} + u_\sigma\,(\sigma - \sigma_0 \cos\hat{\varphi}) + u_\varphi\,\sigma_0\,\sin\hat{\varphi}}{(\hat{x}^2 + \sigma^2 + \sigma_0^2 - 2\sigma\sigma_0 \cos\hat{\varphi})^{5/2}} \\
&\quad \times \Big[(x - x_c)\,\hat{x} + \sigma\,(\sigma - \sigma_0\,\cos\hat{\varphi})\Big] \begin{bmatrix} \hat{x} \\ \sigma\cos\hat{\varphi} - \sigma_0 \\ \sigma\,\sin\hat{\varphi} \end{bmatrix} \mathrm{d}S(\mathbf{x}).
\end{aligned}
\tag{3.8}
$$

To derive integral equations, we apply (3.2) at the particle surface and enforce the aforementioned boundary condition to find

$$
\begin{aligned}
&\mathcal{S}(\mathbf{x}_0, \mathbf{f}, P) + \mathcal{S}(\mathbf{x}_0, \mathbf{f}^D, W) - \mu\,\mathcal{D}^{PV}(\mathbf{x}_0, \mathbf{u}^S, P) - \mu\,\mathcal{D}(\mathbf{x}_0, \mathbf{u}, W) \\
&= -8\pi\mu\,\big[\mathbf{V} + \boldsymbol{\Omega} \times (\mathbf{x}_0 - \mathbf{x}_c) - \mathbf{u}^\infty(\mathbf{x}_0)\big] - 4\pi\mu\mathbf{u}^S(\mathbf{x}_0),
\end{aligned}
\tag{3.9}
$$

where the point $\mathbf{x}_0$ lies on P, and PV denotes the principal-value integral. Next, we apply (3.2) at the wall and note that the principal value of the double-layer potential is identically zero due to the vanishing of the kernel, T_{ijk}, to find

$$
\mathcal{S}(\mathbf{x}_0, \mathbf{f}, P) + \mathcal{S}(\mathbf{x}_0, \mathbf{f}^D, W) - \mu\,\mathcal{D}(\mathbf{x}_0, \mathbf{u}^S, P) = -4\pi\mu\mathbf{u}^D(\mathbf{x}_0),
\tag{3.10}
$$

where the point $\mathbf{x}_0$ lies on W. Complemented with (2.3) and (3.1), the last two equations provide us with a system of six scalar equations for (a) the three components of the traction over the particle surface, and (b) the three components of the disturbance traction over the wall. This three-dimensional problem presents us with significant numerical challenges concerning the discretization of the spherical and planar surfaces bounding the flow and the accurate evaluation of the singular boundary integrals.

3.2 Fourier expansion

A key observation is that the boundaries of the flow, but not the flow itself, are axially symmetric with respect to the x-axis. This geometrical property allows us to simplify the problem by expressing the cylindrical polar components of the left- and right-hand sides of (3.9) and (3.10) in Fourier series with respect to the meridional angle, φ, defined such that $y = \sigma \cos \varphi$ and $z = \sigma \sin \varphi$. The formulation is considerably simplified by observing that each of these Fourier series contains only one non-zero term corresponding to the sine or cosine of the meridional angle.

Since we are interested in a particle moving parallel to the wall and rotating about an axis that is parallel to the wall, we set V_x, V_z, Ω_x, and Ω_y equal to zero and obtain

$$\mathbf{V} + \mathbf{\Omega} \times (\mathbf{x} - \mathbf{x}_c) - \mathbf{u}^\infty = -\Omega_z \sigma \, \cos \varphi \, \mathbf{e}_x + W(x) \, \cos \varphi \, \mathbf{e}_\sigma - W(x) \, \sin \varphi \, \mathbf{e}_\varphi, \tag{3.11}$$

where $\mathbf{e}_x, \mathbf{e}_\sigma, \mathbf{e}_\varphi$, are unit vectors, and

$$W(x) = V_y + \Omega_z \, (x - x_c) - u_y^\infty(x). \tag{3.12}$$

Motivated by this form, we express the velocity as

$$\mathbf{u} = \mathcal{V}_x \, \cos \varphi \, \mathbf{e}_x + \mathcal{V}_\sigma \, \cos \varphi \, \mathbf{e}_\sigma - \mathcal{V}_\varphi \, \sin \varphi \, \mathbf{e}_\varphi, \tag{3.13}$$

and the boundary traction as

$$\mathbf{f} = \mathcal{F}_x \, \cos \varphi \, \mathbf{e}_x + \mathcal{F}_\sigma \, \cos \varphi \, \mathbf{e}_\sigma - \mathcal{F}_\varphi \, \sin \varphi \, \mathbf{e}_\varphi, \tag{3.14}$$

where the coefficients $\mathcal{V}_\alpha$ and $\mathcal{F}_\alpha$ are functions of x and σ. The Cartesian components of the traction are related to the corresponding Fourier coefficients by

$$\mathbf{f} = \mathcal{F}_x \, \cos \varphi \, \mathbf{e}_x + (\mathcal{F}_\sigma \cos^2 \varphi + \mathcal{F}_\varphi \sin^2 \varphi)\mathbf{e}_y + (\mathcal{F}_\sigma - \mathcal{F}_\varphi) \sin \varphi \cos \varphi \, \mathbf{e}_z. \tag{3.15}$$

The y-component of the force and the z-component of the torque exerted on the particle are given by

$$F_y = \pi \int_{C_P} (\mathcal{F}_\sigma + \mathcal{F}_\varphi) \, \sigma \, \mathrm{d}l,$$

$$\tag{3.16}$$

$$T_z = \pi \int_{C_P} \left((x - x_c) \, (\mathcal{F}_\sigma + \mathcal{F}_\varphi) - \sigma \, \mathcal{F}_x \right) \sigma \, \mathrm{d}l,$$

where C_P is the particle contour in the $\varphi = 0$ azimuthal plane consisting of half the xy-plane with $y > 0$, and l is the arc length along C_P. All other components of the force and torque are zero. The Fourier expansion of the tangential component of the traction required for the evaluation of the slip velocity can be expressed in the form

$$\mathbf{n} \times \mathbf{f} \times \mathbf{n} = \mathcal{T}_x \, \cos \varphi \, \mathbf{e}_x + \mathcal{T}_\sigma \, \cos \varphi \, \mathbf{e}_\sigma - \mathcal{T}_\varphi \, \sin \varphi \, \mathbf{e}_\varphi, \tag{3.17}$$

where

$$\mathcal{T}_x = \frac{\sigma}{a^2} (\sigma \mathcal{F}_x - \tilde{x} \mathcal{F}_\sigma), \qquad \mathcal{T}_\sigma = -\frac{\tilde{x}}{a^2} (\sigma \mathcal{F}_x - \tilde{x} \mathcal{F}_\sigma), \qquad \mathcal{T}_\varphi = \mathcal{F}_\varphi, \tag{3.18}$$

over the particle surface, $\tilde{x} = x - x_c$, and

$$\mathcal{T}_x = 0, \qquad \mathcal{T}_\sigma = \mathcal{F}_\sigma, \qquad \mathcal{T}_\varphi = \mathcal{F}_\varphi \tag{3.19}$$

over the wall. Substituting (3.15) in the cylindrical polar components of the single-layer potential, we find

$$\begin{bmatrix} \mathcal{S}_x \\ \mathcal{S}_\sigma \\ \mathcal{S}_\varphi \end{bmatrix} (\mathbf{x}_0) = \int_C \begin{bmatrix} \cos \varphi_0 \left(\Psi_{xx} \mathcal{F}_x + \Psi_{x\sigma} \mathcal{F}_\sigma + \Psi_{x\varphi} \mathcal{F}_\varphi \right) \\ \cos \varphi_0 \left(\Psi_{\sigma x} \mathcal{F}_x + \Psi_{\sigma\sigma} \mathcal{F}_\sigma + \Psi_{\sigma\varphi} \mathcal{F}_\varphi \right) \\ - \sin \varphi_0 \left(\Psi_{\varphi x} \mathcal{F}_x + \Psi_{\varphi\sigma} \mathcal{F}_\sigma + \Psi_{\varphi\varphi} \mathcal{F}_\varphi \right) \end{bmatrix} \mathrm{d}l, \tag{3.20}$$

where the kernel $\Psi_{\alpha\gamma}$ is given in Appendix A.

Next, we substitute (3.13) in the double-layer potential (3.6) and work in a similar fashion to obtain

$$
\begin{bmatrix} \mathcal{D}_x \\ \mathcal{D}_\sigma \\ \mathcal{D}_\varphi \end{bmatrix} (\mathbf{x}_0) = \int_{C_W} \begin{bmatrix} \cos\varphi_0 \left(K_{x\sigma}\mathcal{V}_\sigma + K_{x\varphi}\mathcal{V}_\varphi \right) \\ \cos\varphi_0 \left(K_{\sigma\sigma}\mathcal{V}_\sigma + K_{\sigma\varphi}\mathcal{V}_\varphi \right) \\ -\sin\varphi_0 \left(K_{\varphi\sigma}\mathcal{V}_\sigma + K_{\varphi\varphi}\mathcal{V}_\varphi \right) \end{bmatrix} \, \mathrm{d}\sigma,
\tag{3.21}
$$

where C_W is the line contour of the wall in the azimuthal plane, and the kernel $K_{\alpha\beta}$ is given in Appendix A.

Substituting also (3.13) in (3.8), we obtain

$$
\begin{bmatrix} \mathcal{D}_x \\ \mathcal{D}_\sigma \\ \mathcal{D}_\varphi \end{bmatrix} (\mathbf{x}_0) = -\frac{6}{a} \iint_P \frac{\mathcal{V}_x \cos\varphi\,\hat{x} + \mathcal{V}_\sigma \cos\varphi\,(\sigma - \sigma_0\cos\hat{\varphi}) - \mathcal{V}_\varphi \sin\varphi\,\sigma_0\,\sin\hat{\varphi}}{(\hat{x}^2 + \sigma^2 + \sigma_0^2 - 2\sigma\sigma_0\cos\hat{\varphi})^{5/2}}
$$

$$
\times \left[(x - x_c)\,\hat{x} + \sigma\,(\sigma - \sigma_0\,\cos\hat{\varphi}) \right] \begin{bmatrix} \hat{x} \\ \sigma\cos\hat{\varphi} - \sigma_0 \\ \sigma\,\sin\hat{\varphi} \end{bmatrix} \, \mathrm{d}S(\mathbf{x}).
\tag{3.22}
$$

Carrying out the integrations, we find

$$
\begin{bmatrix} \mathcal{D}_x \\ \mathcal{D}_\sigma \\ \mathcal{D}_\varphi \end{bmatrix} (\mathbf{x}_0) = \int_{C_P} \begin{bmatrix} \cos\varphi_0 \left(L_{xx}\mathcal{V}_x + L_{x\sigma}\mathcal{V}_\sigma + L_{x\varphi}\mathcal{V}_\varphi \right) \\ \cos\varphi_0 \left(L_{\sigma x}\mathcal{V}_x + L_{\sigma\sigma}\mathcal{V}_\sigma + L_{\sigma\varphi}\mathcal{V}_\varphi \right) \\ -\sin\varphi_0 \left(L_{\varphi x}\mathcal{V}_x + L_{\varphi\sigma}\mathcal{V}_\sigma + L_{\varphi\varphi}\mathcal{V}_\varphi \right) \end{bmatrix} \, \mathrm{d}l,
\tag{3.23}
$$

where $L_{\alpha\beta}$ is a derived 3×3 kernel matrix given in Appendix A.

A force balance requires the integral identity

$$
\iint_P T_{ijk}(\mathbf{x}, \mathbf{x}_0)\,n_k(\mathbf{x})\,\mathrm{d}S(\mathbf{x}) = -8\pi c\,\delta_{ij},
\tag{3.24}
$$

where $c = 0$ when $\mathbf{x}_0$ is outside the particle, $c = 1$ when $\mathbf{x}_0$ is inside the particle, and $c = 1/2$ when $\mathbf{x}_0$ is on the surface of the particle. In the third case, the principal value of the integral is implied. Applying this identity for $i = y$, we obtain the derivative identity

$$
a \int_0^\pi (L_{\alpha\sigma} + L_{\alpha\varphi})\,\mathrm{d}\theta = -8\pi c\,(\delta_{\alpha\sigma} + \delta_{\alpha\varphi}),
\tag{3.25}
$$

where θ is the azimuthal angle. The numerical satisfaction of this identity was confirmed with high accuracy as a check on the numerical method.

Now substituting the preceding expressions in (3.2), we obtain an integral representation for the Fourier coefficients,

$$
\mathcal{V}_\alpha^D(\mathbf{x}_0) = -\frac{1}{8\pi\mu} \int_{C_P} \Psi_{\alpha\beta}(\mathbf{x}_0, \mathbf{x})\,\mathcal{F}_\beta(\mathbf{x})\,\mathrm{d}l(\mathbf{x}) - \frac{1}{8\pi\mu} \int_{C_W} \Psi_{\alpha\beta}(\mathbf{x}_0, \mathbf{x})\,\mathcal{F}_\beta^D(\mathbf{x})\,\mathrm{d}l(\mathbf{x})
$$

$$
+ \frac{1}{8\pi} \int_{C_P} L_{\alpha\delta}(\mathbf{x}_0, \mathbf{x})\,\mathcal{V}_\delta^S(\mathbf{x})\,\mathrm{d}l(\mathbf{x}) + \frac{1}{8\pi} \int_{C_W} K_{\alpha\delta}(\mathbf{x}_0, \mathbf{x})\,\mathcal{V}_\delta^D(\mathbf{x})\,\mathrm{d}l(\mathbf{x}),
\tag{3.26}
$$

where the point $\mathbf{x}_0$ lies in the fluid. Substituting this expression in (3.9) and enforcing the boundary conditions, we obtain

$$
\int_{C_P} \Psi_{\alpha\beta}(\mathbf{x}_0, \mathbf{x})\,\mathcal{F}_\beta(\mathbf{x})\,\mathrm{d}l(\mathbf{x}) + \int_{C_W} \Psi_{\alpha\beta}(\mathbf{x}_0, \mathbf{x})\,\mathcal{F}_\beta^D(\mathbf{x})\,\mathrm{d}l(\mathbf{x})
\tag{3.27}
$$

$$
-\frac{a}{\beta_p} \int_{C_P}^{PV} L_{\alpha\delta}(\mathbf{x}_0, \mathbf{x})\,\mathcal{T}_\delta(\mathbf{x})\,\mathrm{d}l(\mathbf{x}) - \frac{a}{\beta_w} \int_{C_W} K_{\alpha\delta}(\mathbf{x}_0, \mathbf{x})\,\mathcal{F}_\delta^D(\mathbf{x})\,\mathrm{d}l(\mathbf{x}) + \frac{4\pi a}{\beta_p}\,\mathcal{T}_\alpha
$$

$$
= -8\pi\mu\,\left(-\Omega_z\,\sigma_0\,\delta_{\alpha x} + W(\mathbf{x}_0)\,\delta_{\alpha\sigma} + W(\mathbf{x}_0)\,\delta_{\alpha\varphi} \right),
\tag{3.28}
$$

where the point $\mathbf{x}_0$ lies on the particle contour, C_P. Finally we substitute (3.26) in (3.10) and find

$$
\int_{C_P} \Psi_{\alpha\beta}(\mathbf{x}_0, \mathbf{x})\,\mathcal{F}_\beta(\mathbf{x})\,\mathrm{d}l(\mathbf{x}) + \int_{C_W} \Psi_{\alpha\beta}(\mathbf{x}_0, \mathbf{x})\,\mathcal{F}_\beta^D(\mathbf{x})\,\mathrm{d}l(\mathbf{x}) - \frac{a}{\beta_p} \int_{C_P} L_{\alpha\delta}(\mathbf{x}_0, \mathbf{x})\,\mathcal{T}_\delta(\mathbf{x})\,\mathrm{d}l(\mathbf{x})
$$

$$
+ \frac{4\pi a}{\beta_w}\,\mathcal{T}_\alpha^D(\mathbf{x}_0) = 0,
\tag{3.29}
$$

where the point $\mathbf{x}_0$ lies on the wall contour, C_W.

3.3 Numerical methods

To solve the integral equations, we divide the boundary contours in the $\varphi = 0$ meridional plane into straight elements over the wall and circular elements over the particle, and approximate the Fourier coefficients with a constant function over each element. For better accuracy, the elements are concentrated near the axis of symmetry with their length increasing geometrically with distance from the axis of symmetry, as depicted in Fig. 1(b). The wall is truncated at a radial distance equal to 48 times the particle separation from the wall, x_c. Applying point collocation at the mid-point of each element, we compile a system of linear equations for the unknown solution vector consisting of the particle and wall traction. In the case of a freely suspended particle, the translational and angular velocities V_y and Ω_z are appended to the vector of unknowns, and two more equations are introduced expressing the vanishing of F_y and T_z.

The elements of the coefficient matrices consisting of element integrals of the single and double-layer potentials are computed by the six-point Gauss–Legendre quadrature. The diagonal components of the dimensionless single-layer kernel, $\Psi_{\alpha\alpha}$, exhibit a logarithmic singularity as the azimuthal angle of the integration point, θ, tends to the azimuthal angle of the evaluation point, θ_0, $\Psi_{xx} \simeq -2\log|\theta - \theta_0|$, $\Psi_{\varphi\varphi} \simeq -2\log|\theta - \theta_0|$, $\Psi_{\varphi\varphi} \simeq -4\log|\theta - \theta_0|$. The $L_{\varphi\varphi}$ component of the particle double-layer kernel, but not any other component, exhibits the singular behavior $L_{\varphi\varphi} \simeq (6/a)\log|\theta - \theta_0|$. These singularities are subtracted out and integrated analytically after the numerical quadrature has been applied.

Basset [9] found that the force exerted on a sphere translating along the y-axis through a quiescent infinite ambient fluid is given by the modified Stokes law $F_y = -6\pi\mu a c_T V_y$, where $c_T = (\beta_p + 2)(\beta_p + 3)$ is a slip-correction coefficient. For a no-slip surface, $c_T = 1$, and for a perfect-slip surface, $c_T = 2/3$. In Sect. 2, we found that the torque exerted on a sphere rotating about the z-axis in a quiescent infinite ambient fluid is given by $T_z = -4\pi\mu a^3 c_R \Omega_z$, where $c_R = \beta_p/(\beta_p + 3)$ is a slip-correction coefficient. For a no-slip surface $c_R = 1$, and for a perfect-slip surface $c_R = 0$. By way of validating the numerical method, we have confirmed these slip correction coefficients. For example, computations in the absence of the wall with $\beta_p = 1$ and 16, 32, and 64 boundary elements around the particle contour, yielded, respectively, $c_T = 0.7546$, 0.7511, and 0.7503, which clearly converge to the exact value, 0.75. As the number of elements is doubled, the numerical error is reduced by a factor of four, revealing that the numerical error is quadratic in the element size.

4 Results and discussion

We have carried out computations for three modular cases to identify (a) the force and torque exerted on a particle that translates parallel to a plane wall in a quiescent fluid, (b) the force and torque exerted on a particle that rotates about an axis that is parallel to a plane wall in a quiescent fluid, and (c) the translational and angular velocities of a freely suspended particle in semi-infinite simple shear flow above a plane wall. The force and torque exerted on a particle that is held stationary in semi-infinite simple shear flow above a plane wall can be deduced readily from these results by linear superposition.

4.1 Translation and rotation in a quiescent fluid

Figure 2 illustrates the effect of the particle and wall slip coefficients for a particle that translates parallel to a plane wall in a quiescent fluid, and Table 1 of Appendix B gives numerical values. In the absence of wall and particle slip, $\beta_w, \beta_p \to \infty$, the numerical results agree with the predictions of Goldman et al. [23] up to the third significant figure. As expected, allowing for slip on the wall or particle surface reduces the drag force for any particle-to-wall separation, x_c/a. The reduction may lower the magnitude of the drag force coefficient below the value of unity corresponding to Stokes' law for a no-slip particle moving in an infinite ambient fluid, even at small particle-wall separations. As β_w approaches zero, the effect of the particle position, x_c/a, on the drag coefficients becomes less

significant. In the case of slip surfaces, the torque is negative in a certain regime of the parametric space determined by the particle and wall slip coefficients. Zero torque occurs under certain conditions where a particle moving under the influence of a force parallel to the wall translates parallel to the wall without rotation, as shown in Fig. 2(b). As the wall and particle surfaces become increasingly slippery, $\beta_w, \beta_p \to 0$, the torque becomes negative for any particle position.

Figure 3 illustrates the effect of the slip coefficients on the distribution of the traction along the particle contour and the distribution of the disturbance traction along the wall contour, both reduced by $\mu V_y/a$, for flow due to a spherical particle translating parallel to a wall at the distance $x_c/a = 1.0453$. Results are shown for three modular cases: (a) $\beta_w = \infty$ and $\beta_p = \infty$ (no-slip wall and particle), (b) $\beta_w = 0.10$ and $\beta_p = \infty$ (slip wall and no-slip particle), and (c) $\beta_w = \infty$ and $\beta_p = 0.10$ (no-slip wall and slip particle). The solid lines representing the x Fourier coefficient of the traction tend to zero at the axis of symmetry in all graphs, while the corresponding σ and φ coefficients of the traction tend to common limits. The latter is necessary for the solution to be single valued. The results confirm that the wall and particle slip has a profound effect on the distribution of the particle and wall shear stress.

Lauga and Squires [21] determined the force on a no-slip sphere translating normal or parallel to a slip wall, $\beta_p = \infty$, at large distances. Their analysis for parallel motion furnishes the asymptotic prediction

$$F_y = -6\pi \mu a V_y \left[1 + \frac{3}{8} \delta [1 - 2 \mathcal{J}(\beta_w/\delta)] + O(\delta^3) \right]^{-1}, \tag{4.1}$$

where $\delta = a/x_c$,

$$\mathcal{J}(x) = -\frac{x}{8}(x+3) + \frac{x}{8}(x+2)^2 e^x E(x) + 2x e^{2x} E(2x), \tag{4.2}$$

and $E(x)$ is the exponential integral (a typographical omission of a factor of two has been incorporated in the above formula.) As x tends to zero or infinity, $\mathcal{J}(x)$ tends, respectively, to zero or 5/2. Replacing the Stokes with the Basset drag formula and keeping only the first-order terms, we find

$$F_y = -6\pi \mu a V_y \frac{\beta_p + 2}{\beta_p + 3} \frac{1}{1 + \frac{3}{8}\delta} + O(\delta^2). \tag{4.3}$$

Yang and Leal [24] determined the force exerted on a small sphere translating parallel to the flat interface between two viscous liquids with viscosities μ and $\lambda\mu$,

$$F_y = -6\pi \mu V_y \left(1 - \Delta + \Delta^2 - \Delta^3 - \frac{1 + 2\lambda}{16(1 + \lambda)} \delta^3 \right) + O(\delta^4), \tag{4.4}$$

where the sphere is immersed in the fluid with viscosity μ, $\Delta = \alpha\delta$ and $\alpha = 3(2 - 3\lambda)/[16(1 + \lambda)]$. Setting $\lambda = 0$ reduces the interface to a free surface with zero shear stress identified with a perfectly slippery wall, $\beta_w = 0$. Setting $\lambda = \infty$ immobilizes the lower fluid and reduces the interface with a solid wall, $\beta_w = \infty$.
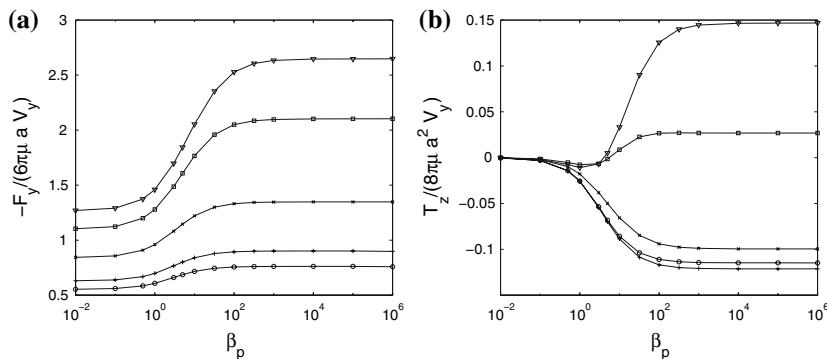

Fig. 2 (**a**) Reduced force, $-F_y/(6\pi \mu a V_y)$, and (**b**) reduced torque, $T_z/(8\pi \mu a^2 V_y)$, exerted on a particle translating parallel to a wall at a distance $x_c/a = 1.0453$, for $\beta_w = \infty$ (*triangles*), 10 (*squares*), 1 (×), 0.1 (+), and 0.01 (o), against the particle slip coefficient, β_p
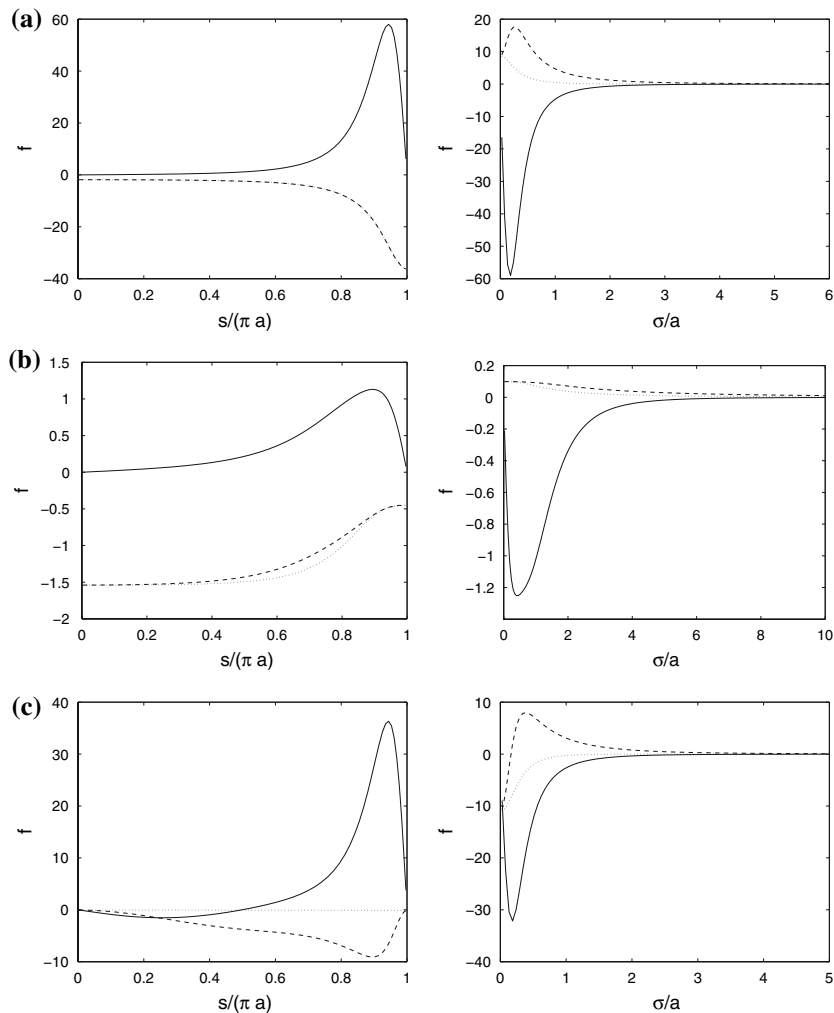
Fig. 3 Flow due to a spherical particle translating parallel to a plane wall at a distance $x_c/a = 1.0453$. The frames on the left show the distribution of the particle traction coefficients $\mathcal{F}_x$ (*solid line*), $\mathcal{F}_\sigma$ (*dashed line*), and $\mathcal{F}_\varphi$ (*dotted line*), plotted against the arc length measured from the axis of symmetry farthest from the wall. The frames on the right show the distribution of the disturbance wall traction coefficients $\mathcal{F}_x^D$ (*solid line*), $\mathcal{F}_\sigma^D$ (*dashed line*), and $\mathcal{F}_\varphi^D$ (*dotted line*), plotted against the arc length measured from the axis of symmetry, for (**a**) $\beta_p = \infty$ and $\beta_w = \infty$, (**b**) $\beta_p = \infty$ and $\beta_w = 0.10$, and (**c**) $\beta_p = 0.10$ and $\beta_w = \infty$

Figure 4(a) shows our numerical results for $\beta_p = \infty$ and several values of β_w. The broken lines represent the second-order predictions stated in (4.1), and the upper solid line represents the asymptotic predictions for a flat free surface, $\lambda = 0$. The agreement between the numerical and asymptotic results is excellent even for small particle-to-wall separations. Figure 4(b) shows corresponding results for $\beta_w = \infty$ and several values of β_p. The broken lines represent the asymptotic predictions stated in (4.3). In this case, the first-order theory is clearly unable to describe with sufficient accuracy the force coefficients, except at very large separations.

Figure 5 illustrates the effect of the particle and wall slip coefficients for a particle rotating about the z-axis that is parallel to the wall, Table 2 of Appendix B gives numerical values, and Fig. 6 illustrates the distribution of the traction coefficients reduced by $\mu\Omega_z$. Once again, we observe the significant effect of the slip velocity. Brenner [25] and Cox and Brenner [26] demonstrated that the torque exerted on a particle in translation along the x-axis, T_z^T, is related to the force exerted on a particle in rotation about the z-axis, F_y^R, by $T_z^T = a\, F_y^R$. Accordingly, the second entry of Table 1 in Appendix B is related to the first entry of Table 2 in the same appendix by $0.0146 \times 8 \approx 6 \times 0.0195$. This symmetry is borne out from our numerical results for arbitrary values of the wall
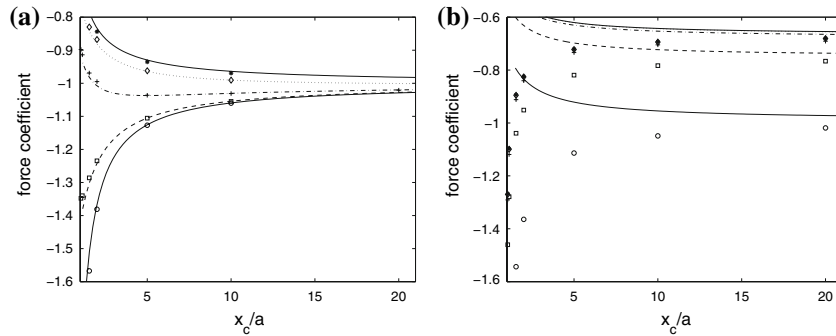
Fig. 4 Force coefficient, $F_y/(6\pi\mu a)$, for $\beta_p = \infty$, and $\beta_w = 100$ (*lower solid line* and *circles*), 1.0 (*dashed line* and *squares*), 0.1 (*dot-dashed line* and *plus signs*), 0.01 (*dotted line* and *diamonds*), and 0.001 (*upper solid line* and *asterisks*). The lower solid line and broken lines represent Lauga and Squires's [21] asymptotic predictions, and the upper solid line represents Yang and Leal's [24] asymptotic predictions for a flat free surface. (**b**) Force coefficient, $F_y/(6\pi\mu a)$, for $\beta_w = \infty$ and $\beta_p = 100$ (*lower solid line* and *circles*), 1.0 (*dashed line* and *squares*), 0.1 (*dot-dashed line* and *plus signs*), 0.01 (*dotted line* and *diamonds*), and 0.001 (*upper solid line* and *asterisks*). The solid lines represent the predictions of the asymptotic expansion (4.3)
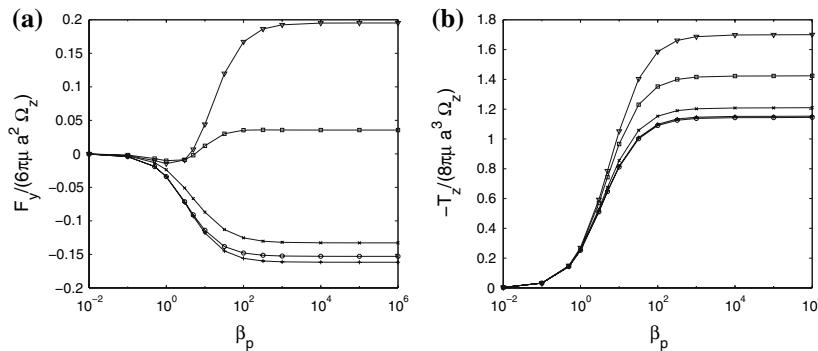

Fig. 5 (**a**) Reduced force, $F_y/(6\pi\mu a^2\Omega_z)$, and (**b**) torque, $-T_z/(8\pi\mu a^3\Omega_z)$, exerted on a particle rotating about the z-axis at a distance $x_c/a = 1.0453$ above a plane wall. The slip coefficient is $\beta_w = \infty$ (*triangles*), 10 (*squares*), 1 ($\times$), 0.1 (+) and 0.01 (*circles*)

and particle slip coefficients. Zero force occurs at the boundaries between contiguous regimes in the slip-coefficient space. Under these specific conditions, a particle moving under the influence of a torque parallel to the wall will rotate without migrating parallel or normal to the wall.

Davis et al. [11] considered the translation and rotation of a sphere whose lower surface is tangential to a plane wall, $x_c = a$, and found that, at large values of β_w and β_p, the force and torque behave as

$$F_y \simeq -\frac{4}{5}\pi\mu a \left(4V_y \log\beta_w - \Omega_z a \log\beta_m\right),$$

(4.5)

$$\Omega_z \simeq -\frac{4}{5}\pi\mu^2 a \left(-4V_y \log\beta_m + 4\Omega_z a \log\beta_p\right),$$

where β_m is the minimum of β_p and β_w. Thus, the force on a translating but non-rotating sphere diverges for a no-slip wall, and the torque on a rotating but non-translating sphere diverges for a no-slip particle. The torque on a translating but non-rotating sphere and the force on a rotating but non-translating sphere is finite either for a no-slip wall or for a no-slip particle, but not for a no-slip wall and a no-slip particle. Davis et al. [11] further developed a series solution for a non-touching sphere and presented numerical results for a slip wall and no-slip
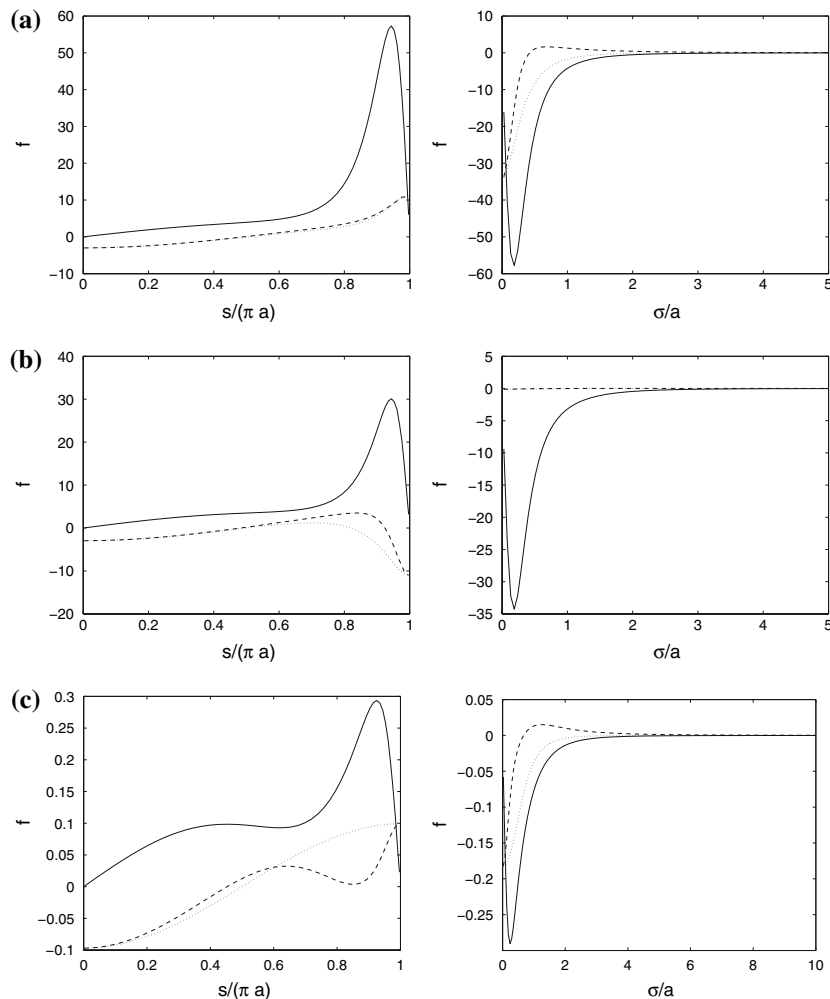
Fig. 6 Counterpart of Fig. 3 for a spherical particle rotating about the z-axis above a plane wall

sphere. Unfortunately, because their data are seemingly plotted on an incorrect scale that does not conform with the asymptotic predictions, we are unable to compare our respective predictions.

To investigate the asymptotic behavior for small sphere-to-wall separations, we introduce the dimensionless gap $\epsilon = (x_c - a)/a$. Figure 7(a, b) shows graphs of the force and torque coefficients for a translating particle with a no-slip surface, and Fig. 7(c, d) shows corresponding results for a rotating particle with a no-slip surface. In both cases, allowing for wall slip yields finite values for the force and torque in the limit of zero gap. When the no-slip condition is imposed on the wall, the force and torque diverge in the limit of zero gap, in agreement with the results of previous authors [11].

O'Neill [27] developed a series solution in bispherical coordinates for no-slip sphere and wall surfaces. The derived expressions are exact, except that the coefficients must be determined numerically from a difference equation. Goldman et al. [23] applied the series solution to calculate the force and torque for dimensionless gaps ϵ as small as 0.0032, and found a logarithmic dependence in the range below 0.0453. O'Neill and Stewartson [28] developed full inner and outer expansions for small gaps. As the gap approaches zero, the force and torque behave like
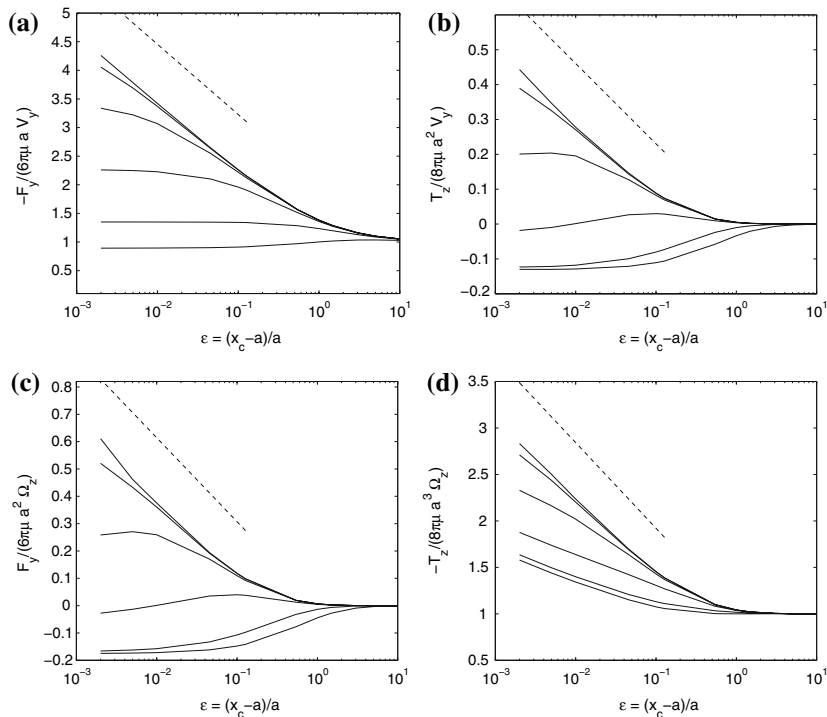
Fig. 7 (**a**) Reduced force, and (**b**) reduced torque on a translating particle with a no-slip surface, $\beta_p = \infty$, plotted against the dimensionless gap, $\epsilon = (x_c - a)/a$, for $\beta_w = 0.1, 1, 10, 100, 1000$, and ∞ (*bold lines*). The dashed line represents the asymptotic solution for small gaps. (**c, d**) Same as (**a, b**) for a rotating particle. Note that the offset of the asymptotic solution is arbitrary

$$\frac{F_y^T}{6\pi\mu a V_y} \sim \frac{8}{15}\log\epsilon, \qquad \frac{T_z^T}{8\pi\mu a^2 V_y} \sim -\frac{1}{10}\log\epsilon. \tag{4.6}$$

In the case of rotation about the z-axis, the asymptotic expansion yields

$$\frac{F_y^R}{6\pi\mu a^2\Omega_z} \sim -\frac{2}{15}\log\epsilon, \qquad \frac{T_z^R}{8\pi\mu a^3\Omega_z} \sim \frac{2}{5}\log\epsilon. \tag{4.7}$$

These predictions, represented by the dashed lines in Fig. 7, are in excellent agreement with our numerical results for no-slip surfaces represented by the bold lines. Consistent with the analytical results, a logarithmic-dependence regime arises when $\epsilon \simeq 0.04$. In principle, the boundary-integral method is able to handle arbitrarily small gaps using a higher number of boundary elements; in practice, increased computational time restricts us to gaps that are greater than 10^{-3} times the particle radius.

4.2 Particle freely suspended in shear flow

In the third case study, we consider the motion of a spherical particle freely suspended in simple shear flow parallel to the wall. Figure 8 illustrates the reduced velocity of translation, $V_y/(kx_c)$, and angular velocity of rotation, $2\Omega_z/k$, and Table 3 of Appendix B gives numerical values. For all particle positions, a minimum translational velocity is observed for no-slip surfaces. In the case of no-slip particle and wall surfaces, $\beta_p, \beta_w \to \infty$, the numerical results represented by the triangles in Fig. 8 agree with the theoretical predictions of Goldman et al. [29] up to the third significant figure. It is interesting that, for the smallest wall slip coefficients, $\beta_w = 0.1$ and 0.01, where the wall nearly behaves like a free surface, the translational particle velocity increases as the particle
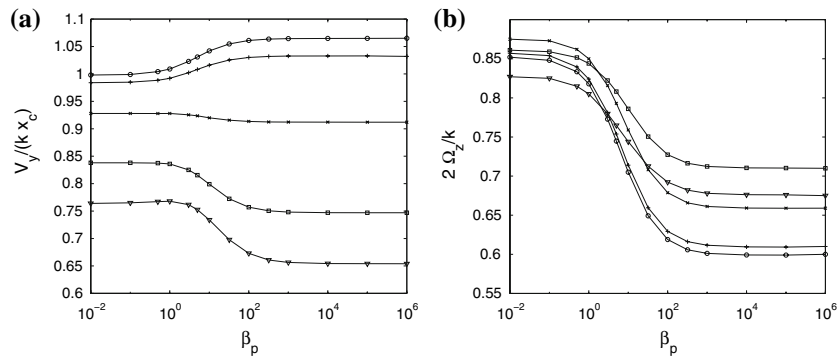
Fig. 8 (**a**) Reduced velocity of translation, $V_y/(kx_c)$, and (**b**) angular velocity of rotation, $2\Omega_z/k$, for a particle freely convected in simple shear flow parallel to the wall at a distance $x_c/a = 1.0453$. The slip coefficient is $\beta_w = \infty$ (*triangles*), 10 (*squares*), 1 ($\times$), 0.1 (+) and 0.01 (o)

surface becomes less slippery, and the reduced velocity $V_y/(kx_c)$ may become greater than unity, which means that the particle may travel faster than the unperturbed fluid velocity evaluated at the particle center. Curiously, a positive shift in the translational velocity is observed for no-slip or nearly no-slip particle surfaces and slippery wall surfaces. However, in wall-bounded flow, there is nothing special about the particle center, and physical intuition suggests that the particle velocity should be less than the unperturbed fluid velocity evaluated at the particle top.

Allowing for slip may either increase or reduce the particle angular velocity, and the dependence on β_w is not necessarily monotonic. Since the ratio $a\Omega_z/V_y$ is well under unity in the limit $x_c \to a$, the particle slips as it rolls over the wall. Figure 9 illustrates the distribution of the particle and wall-traction coefficients and demonstrates once again the important effect of boundary slip.

5 Discussion

We have investigated by analytical and numerical methods the effect of slip velocity on the motion of a particle in infinite fluid and near a plane wall. In the case of infinite flow, we have derived an exact solution using the singularity method, and extracted analytical expressions for the force, torque, and stresslet expressing the particle stress tensor in a dilute suspension. In the case of flow above a plane wall, we have presented numerical results for the force and torque exerted on the particle in the case of translation and rotation, and for the translational and angular velocity in the case of free convection in simple shear flow. Previous authors have considered in great detail corresponding motion for no-slip surfaces and investigated the asymptotic limits of small gaps and large separations for slip surfaces. Our numerical results agree with these predictions in appropriate asymptotic limits, and reveal conditions for particle translation without rotation, and vice versa, under the action of a tangential force or torque near a plane wall. Although we are not able to produce a physical explanation as to why translation without rotation and vice versa may occur near a plane wall due to the slip velocity, we note that a similar situation occurs in the motion of an oblate spheroid with a no-slip surface near a plane wall [30].

The boundary-integral method developed in this paper can handle arbitrary particle shapes subject to the condition of rotational symmetry about an axis that is normal to the wall. Examples include prolate and oblate spheroids and flat disks. However, with the exception of the sphere and the zero-thickness disk, the axisymmetry is lost as these particles tumble under the influence of a shear flow. Moreover, the method can be applied to describe the particle motion in a channel confined between two parallel walls encountered in microfluidics devices. Finally, the method can be applied to describe the motion of a spherical particle near another spherical particle with the same
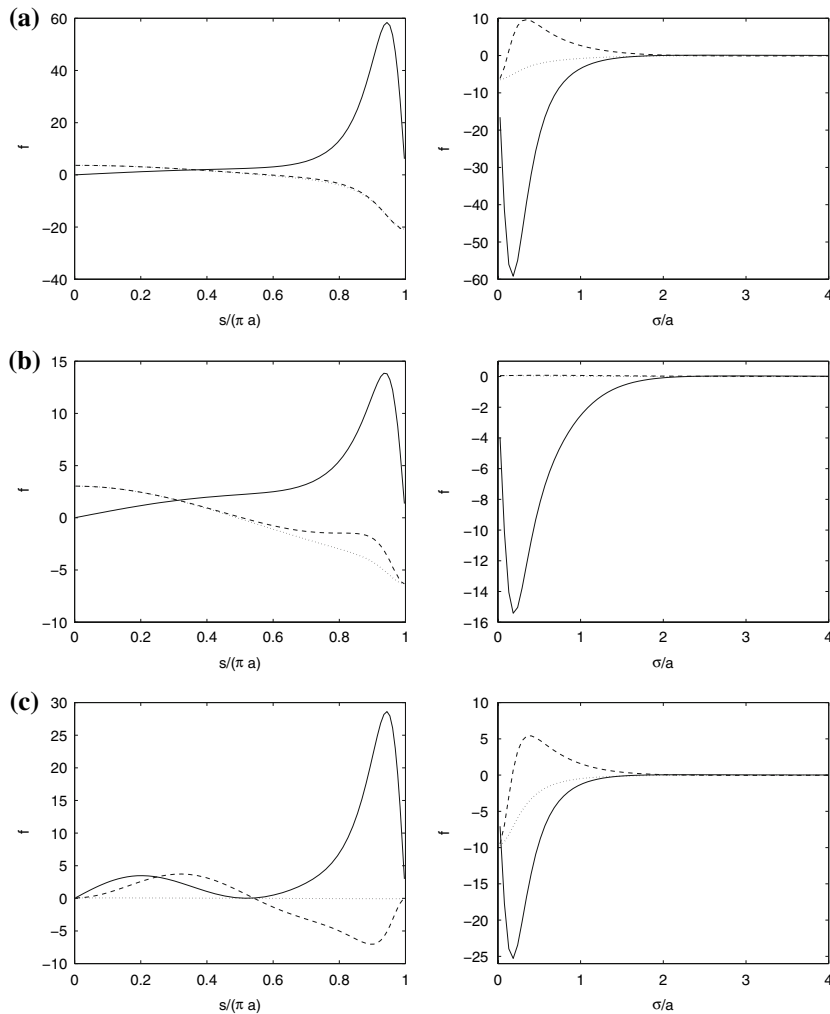
Fig. 9 Counterpart of Fig. 3 for a spherical particle freely convected in simple shear flow above a plane wall

or different radius [31,32]. In all of these configurations, the boundaries of the flow domain are axisymmetric with respect to the axis that passes through the spherical surface or is perpendicular to planar walls.

Appendix A: Fourier kernels of the Stokes potentials

In this Appendix, we give expressions for the kernels of the single- and double-layer potentials for flow in an axisymmetric domain. The kernel of the single-layer potential defined in (3.20) is given by

$$
\Psi_{\alpha\gamma}(\mathbf{x}_0, \mathbf{x}) = \sigma
\begin{bmatrix}
\mathcal{I}_{11} + \hat{x}^2 \mathcal{I}_{31} & \hat{x}(\sigma \mathcal{I}_{31} - \sigma_0 \mathcal{I}_{32}) \\
\hat{x}(\sigma \mathcal{I}_{32} - \sigma_0 \mathcal{I}_{31}) & \mathcal{I}_{12} + (\sigma^2 + \sigma_0^2)\mathcal{I}_{32} - \sigma\sigma_0 (\mathcal{I}_{33} + \mathcal{I}_{31}) \\
\hat{x}\sigma (\mathcal{I}_{30} - \mathcal{I}_{32}) & \mathcal{I}_{10} - \mathcal{I}_{12} + \sigma^2(\mathcal{I}_{30} - \mathcal{I}_{32}) - \sigma\sigma_0 (\mathcal{I}_{31} - \mathcal{I}_{33})
\end{bmatrix}
$$

$$
\begin{matrix}
\hat{x}\sigma_0(\mathcal{I}_{32} - \mathcal{I}_{30}) \\
\mathcal{I}_{10} - \mathcal{I}_{12} + \sigma_0^2 (\mathcal{I}_{30} - \mathcal{I}_{32}) - \sigma\sigma_0 (\mathcal{I}_{31} - \mathcal{I}_{33}) \\
\mathcal{I}_{12} + \sigma\sigma_0 (\mathcal{I}_{31} - \mathcal{I}_{33})
\end{matrix}
\Bigg],
\tag{A1}
$$

where

$$\mathcal{I}_{mn} = \int_0^{2\pi} \frac{\cos^n \omega \, d\omega}{[\hat{x}^2 + \sigma^2 + \sigma_0^2 - 2\sigma\sigma_0 \cos \omega]^{m/2}} = \frac{4w^m}{(4\sigma\sigma_0)^{m/2}} \int_0^{\pi/2} \frac{(2\cos^2 \omega - 1)^n}{(1 - w^2\cos^2 \omega)^{m/2}} \, d\omega, \quad \text{(A2)}$$

and $w^2 = 4\sigma\sigma_0/[\hat{x}^2 + (\sigma + \sigma_0)^2]$. These integrals can be expressed in terms of complete elliptic integrals of the first and second kind that may be evaluated efficiently by iterative methods.

The kernel of the double-layer potential defined in (3.21) is given by

$$K_{\alpha\beta}(\mathbf{x}_0, \mathbf{x})$$
$$= -6\sigma\,\hat{x} \begin{bmatrix} \hat{x}^2\,\mathcal{I}_{51} & \hat{x}(\sigma\,\mathcal{I}_{51} - \sigma_0\,\mathcal{I}_{52}) & \hat{x}\sigma_0\,(\mathcal{I}_{52} - \mathcal{I}_{50}) \\ \hat{x}(\sigma\,\mathcal{I}_{52} - \sigma_0\,\mathcal{I}_{51}) & (\sigma^2 + \sigma_0^2)\,\mathcal{I}_{52} - \sigma\sigma_0\,(\mathcal{I}_{51} + \mathcal{I}_{53}) & \sigma\sigma_0(\mathcal{I}_{53} - \mathcal{I}_{51}) - \sigma_0^2(\mathcal{I}_{52} - \mathcal{I}_{50}) \\ \hat{x}\,\sigma\,(\mathcal{I}_{50} - \mathcal{I}_{52}) & \sigma^2(\mathcal{I}_{50} - \mathcal{I}_{52}) + \sigma\sigma_0(\mathcal{I}_{53} - \mathcal{I}_{51}) & \sigma\sigma_0(\mathcal{I}_{51} - \mathcal{I}_{53}) \end{bmatrix}. \quad \text{(A3)}$$

The kernel in the double-layer potential (3.23) is given by

$$L_{\alpha x}(\mathbf{x}_0, \mathbf{x}) = -\frac{6\sigma\hat{x}}{a} \begin{bmatrix} \hat{x}(\hat{x}\tilde{x} + \sigma^2)\,\mathcal{I}_{51} - \hat{x}\sigma\sigma_0\,\mathcal{I}_{52} \\ -\sigma_0(\hat{x}\tilde{x} + \sigma^2)\,\mathcal{I}_{51} + (\hat{x}\tilde{x}\sigma + \sigma^3 + \sigma\sigma_0^2)\,\mathcal{I}_{52} - \sigma^2\sigma_0\,\mathcal{I}_{53} \\ \sigma\,(\hat{x}\tilde{x} + \sigma^2)\,(\mathcal{I}_{50} - \mathcal{I}_{52}) - \sigma^2\sigma_0\,(\mathcal{I}_{51} - \mathcal{I}_{53}) \end{bmatrix}, \quad \text{(A4)}$$

$$L_{\alpha\sigma}(\mathbf{x}_0, \mathbf{x}) = -\frac{6\sigma}{a} \begin{bmatrix} \hat{x}\left[\sigma\,(\hat{x}\tilde{x} + \sigma^2)\,\mathcal{I}_{51} - \sigma_0\,(\hat{x}\tilde{x} + 2\sigma^2)\,\mathcal{I}_{52} + \sigma\sigma_0^2\,\mathcal{I}_{53}\right] \\ \hline -\sigma\sigma_0\,(\hat{x}\tilde{x} + \sigma^2)\,\mathcal{I}_{51} + (\sigma^2 + \sigma_0^2)\,(\hat{x}\tilde{x} + \sigma^2)\,\mathcal{I}_{52} + \sigma^2\sigma_0^2\,\mathcal{I}_{52} \\ -\sigma\sigma_0\,(\hat{x}\tilde{x} + 2\sigma^2 + \sigma_0^2)\,\mathcal{I}_{53} + \sigma^2\sigma_0^2\,\mathcal{I}_{54} \\ \hline \sigma^2\,(\hat{x}\tilde{x} + \sigma^2)\,\mathcal{I}_{50} + \sigma^2\,(\sigma_0^2 - \hat{x}\tilde{x} - \sigma^2)\,\mathcal{I}_{52} \\ -\sigma\sigma_0\,(\hat{x}\tilde{x} + 2\sigma^2)\,(\mathcal{I}_{51} - \mathcal{I}_{53}) - \sigma^2\sigma_0^2\,\mathcal{I}_{54} \end{bmatrix}, \quad \text{(A5)}$$

and

$$L_{\alpha\varphi}(\mathbf{x}_0, \mathbf{x}) = -\frac{6\sigma}{a} \begin{bmatrix} -\hat{x}\left[\sigma_0(\hat{x}\tilde{x} + \sigma^2)\,(\mathcal{I}_{50} - \mathcal{I}_{52}) - \sigma\sigma_0^2\,(\mathcal{I}_{51} - \mathcal{I}_{53})\right] \\ \hline \sigma_0^2\,(\hat{x}\tilde{x} + \sigma^2)\,\mathcal{I}_{50} - \sigma\sigma_0\,(\hat{x}\tilde{x} + \sigma^2 + \sigma_0^2)\,(\mathcal{I}_{51} - \mathcal{I}_{53}) \\ -\sigma_0^2\,\hat{x}\tilde{x}\,\mathcal{I}_{52} - \sigma^2\sigma_0^2\,\mathcal{I}_{54} \\ \hline \sigma\sigma_0\,(\hat{x}\tilde{x} + \sigma^2)\,(\mathcal{I}_{51} - \mathcal{I}_{53}) - \sigma^2\sigma_0^2\,(\mathcal{I}_{52} - \mathcal{I}_{54}) \end{bmatrix}, \quad \text{(A6)}$$

where $\hat{x} = x - x_0$, and $\tilde{x} = x - x_c$.

Appendix B: Tabulated results

Tables 1–2 give the force and torque exerted on a particle translating or rotating above a plane wall. Table 3 gives the velocity of translation and angular velocity of rotation of a freely suspended particle in simple shear flow above a plane wall.

Table 1 Reduced force, $F_y/(6\pi\mu a V_y)$ (first entry in each cell), and torque, $T_z/(8\pi\mu a^2 V_y)$ (second entry in each cell), for a particle translating parallel to the wall at a distance (a) xc/a=1.5431, (b) 1.1276, and (c) 1.0453

β_p	$\beta_w = \infty$	10	1	0.1	0.01
(a)					
∞	−1.568, 0.0146	−1.515, 9.45e−3	−1.286, −0.0239	−0.969, −0.0578	−0.830, −0.0618
10	−1.386, 8.00e−3	−1.344, 5.07e−3	−1.163, −0.0166	−0.899, −0.0413	−0.778, −0.0448
1	−1.039, −4.46e−5	−1.015, −1.87e−4	−0.907, −4.50e−3	−0.737, −0.0111	−0.653, −0.0124
0.1	−0.912, −1.22e−4	−0.892, −1.19e−4	−0.806, −5.45e−4	−0.668, −1.31e−3	−0.599, −1.48e−3
0.01	−0.896, −1.42e−5	−0.876, −1.36e−5	−0.793, −5.57e−5	−0.659, −1.33e−4	−0.591, −1.50e−4
(b)					
∞	−2.151, 0.0737	−1.906, 0.0286	−1.340, −0.0729	−0.914, −0.1059	−0.773, −0.1029
10	−1.788, 0.0286	−1.631, 0.0122	−1.212, −0.0487	−0.852, −0.0769	−0.727, −0.0761
1	−1.279, −4.32e−3	−1.189, −3.57e−3	−0.948, −0.0130	−0.707, −0.0217	−0.617, −0.0222
0.1	−1.119, −1.02e−3	−1.040, −7.78e−4	−0.845, −1.58e−3	−0.645, −2.60e−3	−0.568, −2.69e−3
0.01	−1.099, −1.11e−4	−1.022, −8.41e−5	−0.831, −1.61e−4	−0.637, −2.65e−4	−0.562, −2.75e−4
(c)					
∞	−2.648, 0.1468	−2.103, 0.0268	−1.348, −0.0995	−0.898, −0.1213	−0.759, −0.1148
10	−2.053, 0.0332	−1.766, 8.71e−3	−1.221, −0.0656	−0.840, −0.0887	−0.716, −0.0857
1	−1.460, −0.0109	−1.279, −7.73e−3	−0.960, −0.0177	−0.698, −0.0256	−0.608, −0.0256
0.1	−1.291, −1.98e−3	−1.123, −1.39e−3	−0.857, −2.16e−3	−0.639, −3.11e−3	−0.561, −3.14e−3
0.01	−1.270, −2.10e−4	−1.104, −1.48e−4	−0.844, −2.21e−4	−0.631, −3.18e−4	−0.554, −3.21e−4

The exponential field is defined as e-n = 10^{-n}

Table 2 Reduced force $F_y/(6\pi\mu a^2 \Omega_z)$ (first entry in each cell) and torque $T_z/(8\pi\mu a^3 \Omega_z)$ (second entry in each cell), for a particle rotating about the z-axis at a distance (a) x_c/a =1.5431, (b) 1.1276, and (c) 1.0453 above a plane wall. The exponential field is defined as e−n=10^{-n}

β_p	$\beta_w = \infty$	10	1	0.1	0.01
(a)					
∞	0.0195, −1.100	0.0126, −1.084	−0.0318, −1.035	−0.0767, −1.004	−0.0821, −0.998
10	0.0106, −0.826	6.74e−3, −0.816	−0.0221, −0.788	−0.0551, −0.770	−0.0598, −0.766
1	7.44e−5, −0.256	−2.35e−4, −0.255	−6.00e−3, −0.252	−0.0148, −0.250	−0.0165, −0.250
0.1	−1.31e−4, −0.0324	−1.32e−4, −0.0323	−7.12e−4, −0.0323	−1.74e−3, −0.0323	−1.97e−3, −0.0323
0.01	1.43e−5, −3.32e−3	1.08e−5, −3.32e−3	−5.82e−5, −3.32e−3	−1.73e−4, −3.32e−3	−2.00e−4, −3.32e−3
(b)					
∞	0.098, −1.388	0.038, −1.270	−0.097, −1.111	−0.141, −1.057	−0.137, −1.049
10	0.038, −0.960	0.016, −0.909	−0.065, −0.824	−0.103, −0.790	−0.102, −0.784
1	−0.0057, −0.265	−0.0047, −0.262	−0.0174, −0.255	−0.0289, −0.251	−0.0296, −0.250
0.1	−1.27e−3, −0.0325	−9.68e−4, −0.0325	−2.08e−3, −0.0323	−3.47e−3, −0.0323	−3.59e−3, −0.0323
0.01	−4.72e−5, −3.33e−3	−3.82e−5, −3.33e−3	−1.84e−4, −3.32e−3	−3.47e−4, −3.32e−3	−3.65e−4, −3.32e−3
(c)					
∞	0.194, −1.700	0.036, −1.424	−0.132, −1.210	−0.158, −1.153	−0.152, −1.145
10	0.044, −1.052	0.012, −0.966	−0.087, −0.855	−0.118, −0.818	−0.114, −0.812
1	−0.0145, −0.270	−0.0102, −0.266	−0.0236, −0.257	−0.0341, −0.252	−0.0340, −0.252
0.1	−2.47e−3, −0.0326	−1.75e−3, −0.0325	−2.84e−3, −0.0324	−4.14e−3, −0.0323	−4.19e−3, −0.0323
0.01	−1.01e−4, −3.33e−3	−8.88e−5, −3.33e−3	−2.55e−4, −3.33e−3	−4.15e−4, −3.33e−3	−4.26e−4, −3.33e−3

Table 3 Reduced velocity of translation, $V_y/(kx_c)$ (first entry in each cell), and angular velocity of rotation, $2\Omega_z/k$ (second entry in each cell), for a particle freely convected in simple shear flow parallel to the wall at a distance (a) x_c/a=1.5431, (b) 1.1276, and (c) 1.0453

	$\beta_w = \infty$	10	1	0.1	0.01
(a)					
$\beta_p = \infty$	0.922, 0.924	0.930, 0.933	0.959, 0.934	0.995, 0.914	1.007, 0.908
10	0.937, 0.938	0.944, 0.946	0.967, 0.948	0.995, 0.933	1.005, 0.928
1	0.956, 0.956	0.961, 0.962	0.977, 0.967	0.994, 0.959	1.001, 0.956
0.1	0.961, 0.961	0.965, 0.967	0.979, 0.972	0.994, 0.966	0.999, 0.964
0.01	0.961, 0.962	0.966, 0.967	0.980, 0.973	0.994, 0.967	0.999, 0.965
(b)					
$\beta_p = \infty$	0.767, 0.780	0.812, 0.807	0.921, 0.777	1.015, 0.730	1.042, 0.719
10	0.817, 0.822	0.850, 0.849	0.932, 0.834	1.006, 0.795	1.027, 0.786
1	0.855, 0.863	0.885, 0.889	0.944, 0.896	0.992, 0.875	1.006, 0.869
0.1	0.859, 0.875	0.890, 0.899	0.946, 0.912	0.988, 0.897	0.999, 0.892
0.01	0.859, 0.876	0.891, 0.901	0.946, 0.914	0.987, 0.899	0.998, 0.895
(c)					
$\beta_p = \infty$	0.654, 0.675	0.747, 0.710	0.912, 0.659	1.032, 0.610	1.065, 0.600
10	0.734, 0.744	0.799, 0.786	0.920, 0.759	1.016, 0.714	1.042, 0.705
1	0.768, 0.805	0.836, 0.844	0.928, 0.850	0.992, 0.824	1.009, 0.818
0.1	0.765, 0.825	0.838, 0.859	0.928, 0.873	0.985, 0.854	0.999, 0.848
0.01	0.764, 0.827	0.838, 0.861	0.928, 0.875	0.984, 0.857	0.998, 0.852

References

1. Vinogradova OI (1999) Slippage of water over hydrophobic surfaces. J Miner Proc 56:31–60
2. Neto C, Evans DR, Bonaccurso E, Butt HJ, Craig VSJ (2005) Boundary slip in Newtonian liquids:a review of experimental studies. Rep Prog Phys 68(12):2859–2897
3. Black WB, Graham MD (2001) Slip, concentration fluctuations and flow instability in sheared polymer solutions. Macromolecules 34:5731–5733
4. Beavers GS, Joseph DD (1967) Boundary conditions at a naturally permeable wall. J Fluid Mech 30:197–207
5. Navier CLMH (1823) Mémoire sur les lois du mouvement des fluides. Mémoires de lAcadémie Royale des Sciences de lInstitut de France VI:389–440
6. Maxwell JC (1879) On stresses in rarefied gases arising from inequalities of temperature. Phil Trans Roy Soc Lond 170:231–256
7. Schaaf SA, Chambre PL (1961) Flow of rarefied gases. Princeton University Press, Princeton
8. Cercignani C (2000) Rarefied gas dynamics. Cambridge University Press, Cambridge
9. Basset AB (1888) A treatise on hydrodynamics. Cambridge University Press, Cambridge; Reprinted by Dover (1961)
10. Hocking LM (1973) The effect of slip on the motion of a sphere close to a wall and of two adjacent spheres. J Eng Math 7:207–221
11. Davis AMJ, Kezirian MT, Brenner H (1994) On the Stokes–Einstein model of surface diffusion along solid surfaces: slip boundary conditions. J Colloid Int Sci 165:129–140
12. Felderhof BU, Jones RB (1978) Faxen theorems for spherically symmetric polymers in solution. Physica A 93:457–464
13. Schmitz R, Felderhof BU (1978) Creeping flow about a sphere. Physica A 92:423–437
14. Felderhof BU, Jones RB (1986) Hydrodynamics scattering theory of flow about a sphere. Physica A 136:77–98
15. Keh HJ, Chen SH (1996) The motion of a slip spherical particle in an arbitrary Stokes flow. Eur J Mech B/Fluids 15:791–807
16. Mohan A, Brenner H (2005) An extension of Faxen's laws for nonisothermal flow around a sphere. Phys Fluids 17:038107
17. Wen SB, Lai CL (2003) Theoretical analysis of flow passing a single sphere moving in a micro-tube. Proc R Soc Lond A 459:495–526
18. Palaniappan D, Daripa P (2001) Interior Stokes flows with stick-slip boundary conditions. Physica A 297:37–63
19. Elasmi L, Feuillebois F (2001) Green function for a Stokes flow near a porous slab. ZAMP 81:743–742
20. Elasmi L, Feuillebois F (2003) Integral equation method for creeping flow around a solid body near a porous slab. Quart J Mech Appl Math 56:163–185
21. Lauga E, Squires TM (2005) Brownian motion near a partial-slip boundary: a local probe of the no-slip condition. Phys Fluids 17:103102
22. Pozrikidis C (1992) Boundary integral and singularity methods for linearized viscous flow. Cambridge University Press, New York
23. Goldman AJ, Cox RG, Brenner H (1967) Slow viscous motion of a sphere parallel to a plane wall–I Motion through a quiescent fluid. Chem Eng Sci 22:637–651

24. Yang SM, Leal LG (1984) Particle motion in Stokes flow near a plane fluid-fluid interface. Part 2. Linear shear and axisymmetric straining flows. J Fluid Mech 149:275–304
25. Brenner H (1964) The Stokes resistance of an arbitrary particle–II. Chem Eng Sci 19:599–629
26. Cox RG, Brenner H (1967) Effect of finite boundaries on Stokes resistance of an arbitrary particle. 3. Translation and rotation. J Fluid Mech 28:391–411
27. O'Neill ME (1964) A slow motion of viscous liquid caused by a slowly moving sphere. Mathematika 11:67–74
28. O'Neill ME, Stewartson K (1967) On the slow motion of a sphere parallel to a nearby plane wall. J Fluid Mech 27:705–724
29. Goldman AJ, Cox RG, Brenner H (1967) Slow viscous motion of a sphere parallel to a plane wall. Part II:Couette flow. Chem Eng Sci 22:653–660
30. Pozrikidis C (1994) The motion of particles in the Hele-Shaw cell. J Fluid Mech 261:199–222
31. Luo H, Pozrikidis C (2007) Interception of two spheres with slip surfaces in linear Stokes flow. J Fluid Mech 581:129–156
32. Pozrikidis C (2007) Interception of two spherical particles with arbitrary radii in simple shear flow. Acta Mech Accepted